Chapter-III

3.1 Introduction

As discussed in Section 1.12 of Chapter I, the crystal structure and the exact location of the MPB region of BNT-PT solid solution at room temperature are controversial. In an early study, Zhang et al. (2012) have reported the phase transition from the rhombohedral (R) to tetragonal (T) phase. These authors report the presence of very narrow MPB in the composition range 0.46 to 0.48 with coexisting R+T structures. However, the comprehensive structural study has not been done. Choi et al. (2005) have reported the phase diagram of BNT-PT using the results of calorimetric and dielectric studies. These authors have reported the phase transition from pseudocubic rhombohedral phase with space group $R\bar{3}m$ to tetragonal phase with space group P4mm. The MPB is reported to lie around x=0.49 [Choi et al. (2005)]. Kang et al. (2012) have shown that the structure of BNT-PT is very sensitive to compositional fluctuations across MPB. Significant modification in the crystal structure of BNT-PT is observed by the addition of excess amount of PbO, NiO, TiO_2 and Bi_2O_3 during synthesis. Doping of 1 to 3 mole % of PbO, NiO and Bi_2O_3 transforms the coexistence in the MPB region into tetragonal structure. The effect is less prominent after the doping of 1 to 5 mole% of TiO_2 [Kang et al. (2013)]. Further, doping of small amount of Sr at Pb-site improves the problem of leakage current and reduces the loss [Kang et al. (2012)]. However, no detailed Rietveld structural analysis has been done on BNT-PT to determine the structural parameters and the structure of the MPB phase in the earlier studies. The controversial report about the structure

and the location of the MPB of BNT-PT makes it essential to carry out a comprehensive structural study on this material using Rietveld method for better understanding of structure property correlations.

In this Chapter, we attempt to resolve the existing controversies regarding the crystal structures of (1-x)BNT-xPT at room temperature. We have refined the room temperature crystal structure of BNT-PT solid solution across MPB in the composition range of $0.35 \leq x \leq 0.55$ at close compositional interval (0.01) using Rietveld method. We find that a monoclinic phase space group Pm co-exists with the tetragonal phase (P4mm) in the MPB region. We have also determined precisely the stability region of various crystallographic phases around the MPB at room temperature.

3.2 Experimental Details

Details of sample preparation are described in Chapter II. For the structural study, the green pellets were kept at 500^0C for 10 hours to burn out the binder and then sintered at 950^0C for 3 hours in a closed alumina crucible. The calcined powder of the same composition was kept inside the closed crucible as sacrificial powder for preventing the loss of volatile Bi and Pb oxides during sintering. For x-ray diffraction (XRD) measurements, sintered pellets were crushed into fine powder and then annealed at 500^0C for 10 hours to remove the strains introduced during crushing. XRD measurement was carried out using an 18kW rotating Cu-anode based Rigaku (Japan) powder diffractometer operating in the Bragg-Brentano geometry and fitted with a curved crystal graphite monochromator. Rietveld structure refinements were carried out using

FULLPROF-Suite [Carvajal (2011)]. The compositions close to the MPB exhibited anisotropic peak broadening. The anisotropic peak shape function suggested by Stephens and also incorporated in the Fullprof program was used to refine the structure [Stephens (1999)].

3.3 Introduction to the Rietveld Refinement Method

The Rietveld method is extensively recognised and widely accepted for the precise structural analysis of crystalline materials. In recent years this method has been used as a vital tool for quantitative phase analysis in the areas of physics, chemistry, materials science and geology. The Rietveld analysis program was developed by H. M. Rietveld [Rietveld (1967); Rietveld (1969)] to analyse of crystal structure of crystalline materials using neutron, synchrotron or X-ray powder diffraction data [Malmros and Thomas (1977); Khattak and Cox (1977); Young (1993)]. Rietveld method does not predict the crystal structure but it fits an approximated structural model to the experimental data. So, understanding of basic crystal structure is essential for fitting the experimental data. If the starting structural model is correct then true crystal structure can be determined by the refinement. Least squares approach is used to refine the true structure in Rietveld method. In the least square approach theoretical XRD profile is generated using the starting structural model and tried to match with the experimental XRD profile. By adjusting the structural and instrumental parameters in the starting structural model, the difference between theoretical and experimental pattern is minimised to an acceptable level. In the Rietveld method, the quantity used to minimize is χ^2 [Young (1993)]. χ^2 is the weighted sum of

squared differences between the observed ($y_{o,i}$) and calculated ($y_{c,i}$) intensity values at the i^{th} step of the XRD pattern.

$$\chi^2 = \sum w_i . (y_{o,i} - y_{c,i})^2 \quad \ldots\ldots\ldots\ldots\ldots\ldots \quad (3.1)$$

where, $w_i = 1/\sigma_{o,i}^2$, $\sigma_{o,i}^2$ is the variance of the observed data $y_{o,i}$ [Young (1993); Prince (2004); David (2004); Toby (2006)]. Various agreement factors are used in Rietveld method to ascertain the quality of fit between experimental and calculated patterns quantitatively. The agreement factor weighted profile R-factor (R_{wp}) which reflect the goodness of fit between experimental and calculated XRD patterns is the square root of the quantity minimised, divided by the weighted intensities [Young (1993); Toby (2006)] defined as

$$R_{wp}^2 = \sum w_i . (y_{o,i} - y_{c,i})^2 / \sum w_i . (y_{o,i})^2 \ldots\ldots \quad (3.2)$$

Other agreement factor used in Rietveld fit is expected R-factor (R_{exp}). If N is number of data points, R_{exp} is written as [Young (1993), Toby (2006)]

$$R_{exp}^2 = N/ \sum w_i . (y_{o,i})^2 \quad \ldots\ldots\ldots\ldots\ldots\ldots \quad (3.3)$$

χ^2 can be directly obtained from the expected and weighted profile R-factors

$$\chi^2 = R_{wp}/R_{exp} \ldots\ldots\ldots\ldots\ldots\ldots\ldots \quad (3.4)$$

The value of χ^2 should be never less than one. However, if the fit results in $\chi^2 < 1$ which implies that $\langle (y_{o,i} - y_{c,i})^2 \rangle$ is less than $\sigma^2(y_{o,i})$. This may occur due to the fact that standard uncertainties for the data are overestimated or additional parameters have been introduced so that the model is fitting the noise. Such types

of features are common in powder diffraction [Toby (2006)]. However, if χ^2 >>1, then it may be that the model is logical but the standard uncertainty values are underestimated. Other reason may be that the model is imperfect because there are errors in the data that do not correspond to the model or finally the model is incorrect [Toby (2006)]. On the other hand, the values of χ^2 nearly equal to 1 does not necessarily means that the fit is correct. This can be achieved by taking different models which can give equivalent fits due to insufficient experimental data [Toby (2006)].

Different types of profile functions have been suggested to define the peak shape of calculated XRD pattern in the Rietveld method. Pseudo-Voigt is one of the widely used functions by crystallographers. Pseudo-Voigt function (pV(x)) is the linear combination of Lorentzian (L(x)) and Gaussian (G(x)) functions which can be written as

$$pV(x)= \eta L(x) + (1- \eta)G(x) \ldots\ldots\ldots\ldots\ldots\ldots \quad (3.5)$$

The width of the x-ray diffraction peaks (which is also called as full width at half maximum (FWHM)) is a significant parameter during crystal structure analysis. FWHM is a variable parameter and depend upon the diffraction angle 2θ in addition to other instrumental factors. Gaussian component [Cagliotiet al. (1958); Mccusker et al. (1999); Carvajal (2001)] of the FWHM is modelled according to equation (3.6) as

$$FWHM= U\tan^2\theta + V\tan\theta + W\ldots\ldots\ldots\ldots\ldots \quad (3.6)$$

Where, U, V and W are refinable parameters. Lorentzian component is modelled [Cagliotiet al. (1958); Mccusker et al. (1999); Carvajal (2001)] by equation (3.7)

$$FWHM = X\tan\theta + Y/\cos\theta \quad (3.7)$$

The values of U, V and W parameters are fixed for the specific diffractometer and nearly constant unless there is no line broadening from the sample due to particle size and/ or strain.

3.4 Details of the Rietveld Refinement of (1-x)BNT-xPT

Rietveld structure refinements were carried out using FULLPROF package [Carvajal (2011)]. The compositions close to the MPB exhibited anisotropic peak broadening similar to Pb-based other MPB ceramics [Singh et al. (2006); Singh et al. (2007)]. The anisotropic peak shape function suggested by Stephens (1999) and also incorporated in the Fullprof program was used to refine the structure. In the refinement process the background was modelled using 5^{-th} order polynomial while the peak shapes were modeled by Pseudo-Voigt function. Occupancy parameters of all the ions were fixed at the nominal composition during refinement. Zero correction, scale factor, background, half width parameters (U, V and W), lattice parameters, positional coordinates and thermal parameters were varied during the refinement. The isotropic thermal parameter for Pb/Bi ions was very high. In view of this, anisotropic thermal parameters were used for A-site cations (Pb/Bi) for all the compositions except for the cubic compositions with $x \leq 0.40$.

The Wyckoff positions and the asymmetric unit for the various space groups used during the Rietveld refinement of structures of BNT-PT system in the present work are given below:

(i) In the cubic structure with $Pm\bar{3}m$ space group, the occupancy of Bi/Pb ions were fixed at 1(a) sites (0, 0, 0), Ti/Ni ions at 1(b) sites (1/2, 1/2, 1/2) and oxygen ions at 3(c) sites (1/2, 1/2, 0).

(ii) For the refinement of the rhombohedral structure with space group $R\bar{3}m$, we used the hexagonal unit cell having lattice parameters $a_H=b_H=\sqrt{2}a_R$ and $c_H=\sqrt{3}a_R$, where a_R corresponds to rhombohedral lattice parameter. To fix the origin for the rhombohedral structure, the z-coordinate of O ion was fixed at 1/6. In the asymmetric unit of the rhombohedral structure with $R\bar{3}m$ space group, Bi/Pb and Ti/Ni ions occupy 3(a) sites at (0, 0, z) and O ion at the 9(b) site at (x, 2x, z).

(iii) In the tetragonal structure with P4mm space group, the occupancy of Bi/Pb ions were fixed at 1(a) sites (0, 0, z), Ti/Ni and O_I in 1(b) sites at (1/2, 1/2, z), and O_{II} in 2(c) sites at (1/2, 0, *z*).

(iv) For the monoclinic structure with space group Cm, the occupancy of Bi/Pb, Ti/Ni and O_I were fixed in 2(a) sites at (x, 0, z) and O_{II} in 4(b) sites at (x, y, z).

(v) For the monoclinic phase with space group Pm, the occupancy of Bi/Pb and O_I ions were fixed in 1(a) sites at (x, 0, *z*), Ti/Ni, O_{II} and O_{III} in 1(b) sites at (x, 1/2, *z*).

3.5 Results and Discussion

3.5.1 Structure and Location of the MPB in (1-x)BNT-xPT at Room Temperature

Fig.3.1 shows the powder XRD profiles of the (200), (220) and (222) pseudocubic reflections for BNT-PT solid solution in the composition range x=0.35 to 0.55. It is evident from Fig.1 that there is no splitting in the XRD profiles for the compositions with $x \leq 0.40$ and all the XRD profiles are singlet, which suggest the cubic structure for these compositions. For the composition with x=0.41, a tail appears towards the lower 2θ side for (200) pseudocubic reflection and on the higher 2θ side for (220) pseudocubic reflection. The (222) pseudocubic profile is also significantly broader than that for x=0.40 and an asymmetry is observed on the lower 2θ side. This suggests that the structure of the composition with x=0.41 is neither tetragonal nor rhombohedral but either coexistence of these two or a monoclinic/orthorhombic phase reported in several MPB systems [Kuwata et al. (1981); Noheda et al. (1999); Singh and Pandey (2001); Orauttapong et al. (2002); Singh and Pandey (2003); Singh et al. (2007)]. If the dominant phase has a monoclinic structure then the coexistence of monoclinic phase with tetragonal phase may be expected in the PT rich compositions. For $x \geq 0.50$, the (200) and (220) profiles appear as doublet and (222) profile as a singlet, which suggests that the dominant phase for these compositions has tetragonal structure. It can be seen from Fig.1 that the (002) profile is significantly broader than that of (200) for the compositions with x=0.49 and 0.50. The anisotropic peak shape function suggested by Stephens

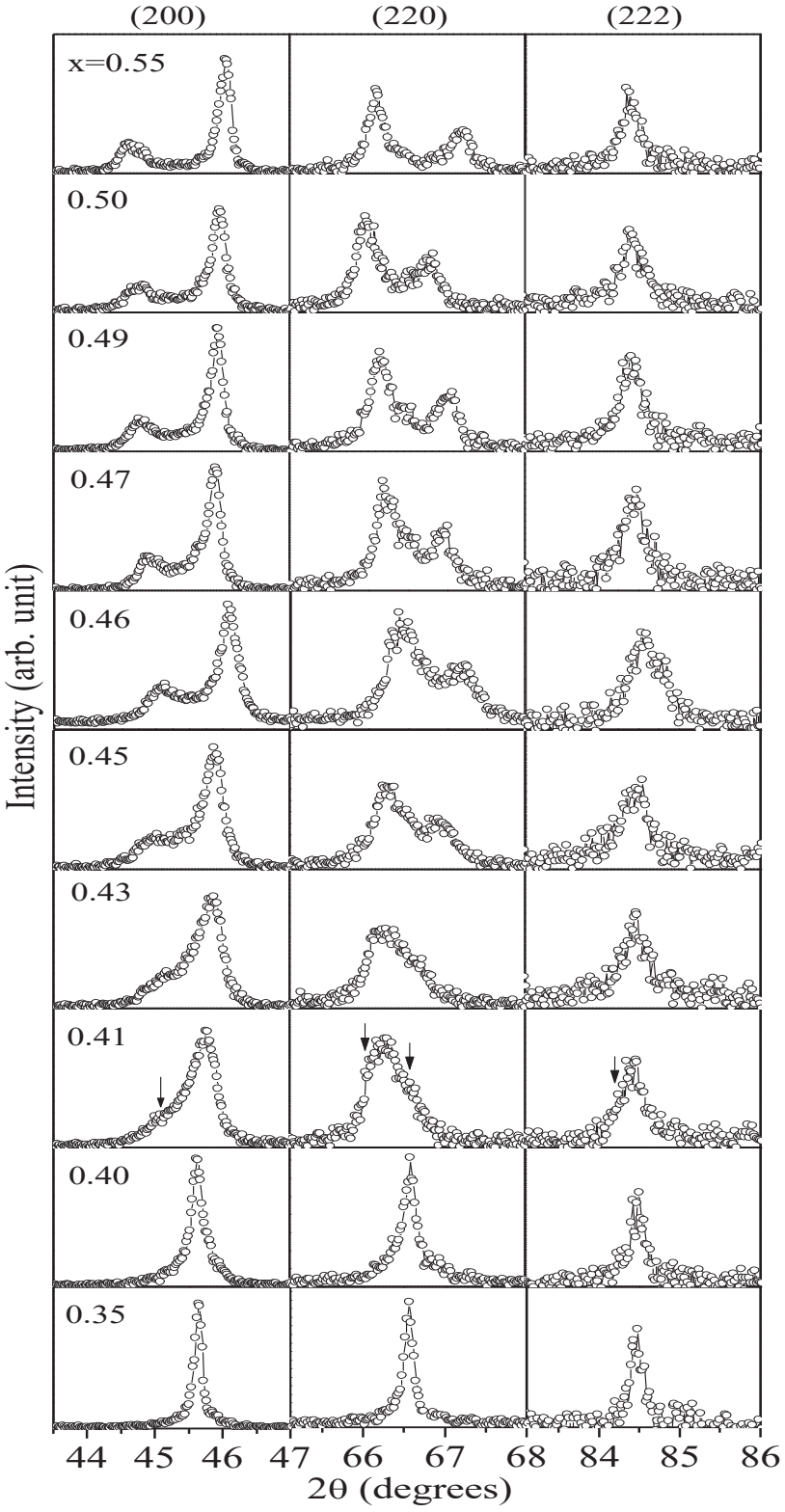

Fig.3.1. Evolution of (200), (220) and (222) pseudocubic XRD profiles for various compositions of BNT-PT at room temperature.

(1999) is used to get the satisfactory fit for the Rietveld structure refinement of the compositions close to the MPB. We have also introduced the anisotropic peak shape function during the Rietveld structure refinement of BNT-PT solid solution. Fig.2 depicts the variation of the FWHM for (222) pseudocubic profile as a function of composition (x) in the composition range $0.35 \leq x \leq 0.55$. The (222) profile should be a singlet in the tetragonal and cubic structures, whereas more than one reflection should appear for the compositions in phase coexistence region or with monoclinic structure. As can be seen from Fig.2, the FWHM is significantly enhanced for the composition range $0.41 \leq x < 0.49$, while it decreases on the either side. This clearly suggests the presence of lower symmetry phase or a phase coexistence region for these compositions [Pandey and Singh (2014); Singh et al. (2009)]. The phase coexistence region for BNT-PT reported by earlier researchers is in broad agreement with the present work [Hu et al. (2010); Choi et al. (2005); Kang et al. (2012)]. However, the earlier researchers have reported the coexistence of rhombohedral and tetragonal structure. As shown in Chapter IV, the large broadening of the (222) profile transform into clear splitting in the MPB compositions corresponding to monoclinic structure on the application of electric field poling. In the subsequent Sections, we present the results of Rietveld analysis to unambiguously determine the structure of BNT-PT ceramics across the MPB.

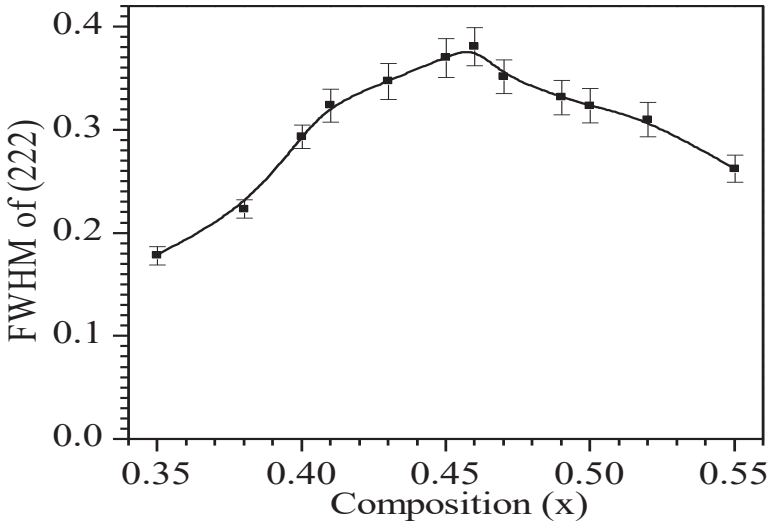

Fig.3.2. Composition dependent variation of full width at half maxima (FWHM) of (222) pseudocubic reflection for (1-x)BNT-xPT solid solution with x=0.35, 0.38, 0.40, 0.41, 0.43, 0.45, 0.46, 0.47, 0.49, 0.50, 0.52 and 0.55.

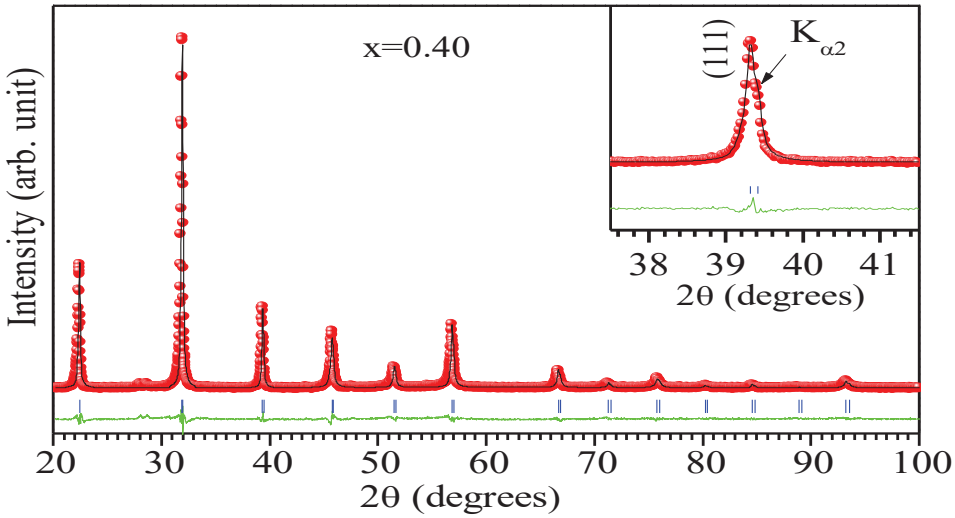

Fig.3.3. Experimentally observed (dots), theoretically calculated (continuous line) and their difference (continuous bottom line) profiles for (1-x)$Bi(Ni_{1/2}Ti_{1/2})O_3$-x$PbTiO_3$ with x=0.40 obtained after Rietveld analysis of the powder XRD data using cubic ($Pm\bar{3}m$) structure. The vertical tick-marks above the difference plot show the peak positions. The inset illustrates the goodness of fit for (111) profile.

3.5.2 Rietveld Analysis of the X-ray Powder Diffraction Data

In this Section, we present the results of Rietveld analysis to unambiguously determine the structure of (1-x)BNT-xPT solid solutions across the MPB.

3.5.2.1 Cubic Structure with Space Group $Pm\bar{3}m$ ($x \leq 0.40$)

As discussed in Section 3.5.1, the XRD profiles for the composition with $x \leq 0.40$ do not show any clear splitting and appear to be singlet. In view of this, we refined the structure of these compositions using cubic symmetry with space group $Pm\bar{3}m$. Rietveld fit for the BNT-PT solid solution with x=0.40 using cubic structure (space group $Pm\bar{3}m$) is shown in Fig.3.3. The inset shows the goodness of fit for the (111) profile. It is clear from the inset to Fig.3.3 that (111) profile is a singlet and no asymmetry or splitting is observed in lower 2θ side, as observed in the rhombohedral phase of other MPB systems like PZT, PMN-PT etc [Kuwata et al. (1981); Noheda et al. (1999); Singh et al. (2007); Singh and Pandey (2001); Orauttapong et al. (2002); Singh and Pandey (2003)]. Thus the structure of BNT-PT compositions with $x \leq 0.40$ is cubic in the $Pm\bar{3}m$ space group. Very high isotropic thermal parameters were observed for the A-site (~ 4.0(7)$Å^2$), B-site (~ 2.3(1)$Å^2$) cations and O anions (~ 6(4)$Å^2$). The large values of thermal parameters suggest that the system is highly disordered. The Rietveld structure refinement for the composition with x=0.35 also confirms the cubic structure with space group $Pm\bar{3}m$.

3.5.2.2 Monoclinic Structure with Space Group Pm ($0.41 \leq x < 0.43$)

As discussed in Section 3.5.1, the XRD profile for the composition range $0.41 \leq x < 0.43$ exhibit asymmetric tail and broadening suggesting presence of a lower symmetry structure. In order to determine the structure for the composition range x=0.41 to 0.43, we carried out the Rietveld analysis of the structure considering different plausible space groups viz. monoclinic space group Cm and Pm, and rhombohedral space group $R\bar{3}m$. The Rietveld fits for the (200), (220) and (222) pseudocubic reflections for the composition with x=0.41 are shown in Fig.3.4. The value of χ^2 is also given in the right panel of Fig.3.4 for various structural models. The best fit between the experimentally observed and theoretically calculated XRD profiles is obtained for the space group Pm. Although, the satisfactory fit is found for the (200) and (220) profiles using space group Cm but very poor fit is obtained for the (222) pseudocubic profile, as can be seen from the difference plot. It is further corroborated with the lowest value of χ^2 obtained for the Pm space group in the composition range 0.41-0.43. In contrast, the rhombohedral phase with space group ($R\bar{3}m$) gives very poor fit for all the profiles. Consideration of minor coexisting tetragonal phase along with the monoclinic 'Pm' phase improves further the Rietveld fit and gives lower χ^2. Thus, the structure is predominately monoclinic with space group Pm for the composition range x=0.41-0.43. The refined structural parameters and agreement factors are listed in Table 3.1 for the composition range $0.41 \leq x < 0.43$ using the monoclinic structure with Pm space group.

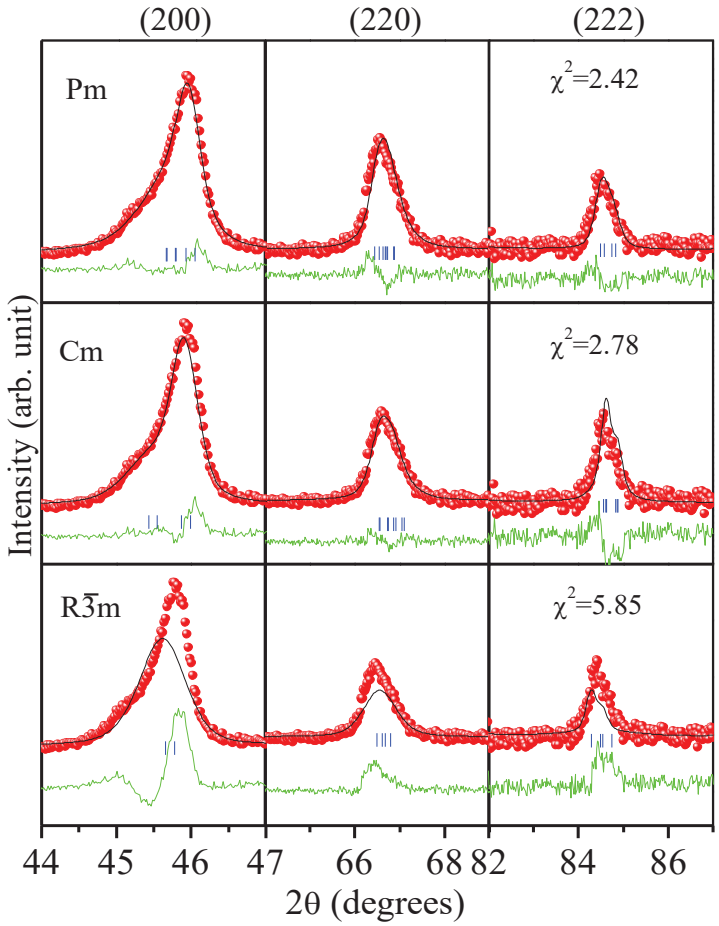

Fig.3.4. Experimentally observed (dots), theoretically calculated (continuous line) and their difference (continuous bottom line) profiles for (1-x)Bi($Ni_{1/2}Ti_{1/2}$)O_3-x$PbTiO_3$ with x=0.41 obtained after Rietveld analysis of the powder XRD data using monoclinic (Pm), monoclinic (Cm) and Rhombohedral ($R\bar{3}m$) structures. The vertical tick-marks above the difference plot show the peak positions.

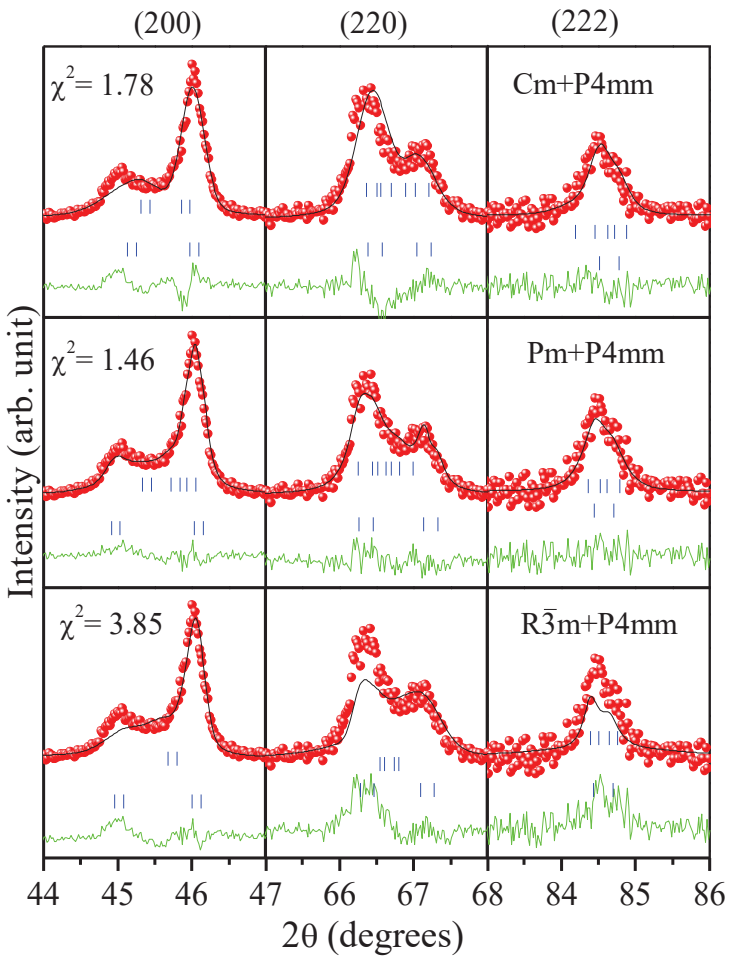

Fig.3.5. Experimentally observed (dots), theoretically calculated (continuous line) and their difference (continuous bottom line) profiles for (1-x)Bi($Ni_{1/2}Ti_{1/2}$)O_3-x$PbTiO_3$ with x=0.46 obtained after Rietveld analysis of the powder XRD data using (Cm+P4mm), (Pm+P4mm) and (R$\bar{3}$m+P4mm) structures. The vertical tick-marks above the difference plot show the peak positions.

3.5.2.3. Phase Coexistence Region with Pm and P4mm Space Groups (0.43≤x≤0.49)

As discussed in Section 3.5.1 and shown in Fig.3.2, the FWHM for the (222) pseudocubic profile is significantly enhanced for the intermediate compositions suggesting presence of lower symmetry phase or phase coexistence region. In order to determine the structure of these compositions, we carried out the Rietveld analysis of the powder XRD data using various plausible structures. Consideration of lower symmetry single phase monoclinic Cm, monoclinic Pm and orthorhombic Bmm2 structures do not give satisfactory fit. This suggests that a coexisting tetragonal structure is also needed to be considering in the structure refinement. In view of this, we considered various plausible phase coexistence models for structure refinement of these compositions. The Rietveld fit for (200), (220) and (222) pseudocubic reflections using (Pm+P4mm), (Cm+P4mm) and ($R\bar{3}m$+P4mm) structural models are shown in Fig.5 for x=0.46. It is evident from Fig.5 that the Rietveld fit for the $R\bar{3}m$ phase coexisting with the P4mm phase is very poor. The fit for the (Cm+P4mm) is better than ($R\bar{3}m$+P4mm) model, but significantly inferior than that obtained for (Pm+P4mm) model. The coexistence of (Pm+P4mm) provides the lowest value of χ^2, also. Thus, the structure of BNT-PT in the phase coexistence region consists of coexisting monoclinic (Pm space group) and tetragonal (P4mm space group) structures for the composition range 0.43≤x≤0.49 rather than ($R\bar{3}m$+P4mm) as reported by earlier authors [Choi et al. (2005); Zhang et al. (2012)].

3.5.2.4. Tetragonal Structure with Space Group P4mm (x≥0.50)

As discussed in Section 3.5.1, the compositions with x≥0.50 exhibit well resolved doublets for (200) and (220) profiles while the broadening for (222) profile is reduced. This suggest that the structure of these compositions can be predominately tetragonal similar to that of the end component $PbTiO_3$. The Rietveld fit for the composition with x=0.55 using tetragonal structure with space group P4mm is shown in Fig.3.6. The fit is quite satisfactory which suggests that the structure is indeed tetragonal (P4mm) for this composition. As observed for the tetragonal compositions close to the MPB for other MPB ceramics like PZT [Singh et al. (2007)] and PMN-PT [Singh and Pandey (2003)], consideration of small coexisting monoclinic phase further improves the fit. The refined structural parameters and the agreement factors are listed in Table 3.1 for x≥0.50 using the tetragonal structure (P4mm) as major phase.

3.5.2.5. Variation of Lattice Parameters with Composition

Fig.3.7 depicts the variation of lattice parameters with composition for BNT-PT solid solution. For cubic compositions, the lattice parameter 'a' has slightly decreasing trend with increasing PT concentration and corresponds to monoclinic a_m parameter for higher compositions. Monoclinic cell parameter c_m increases while a_m and b_m decrease with increasing PT concentration inside the MPB region. The tetragonal cell parameter c_t increases while a_t decreases with increasing PT concentration. The monoclinic angle (β) increases with increasing the major monoclinic phase (Pm) and start decreasing with increasing tetragonal phase fraction outside the MPB region.

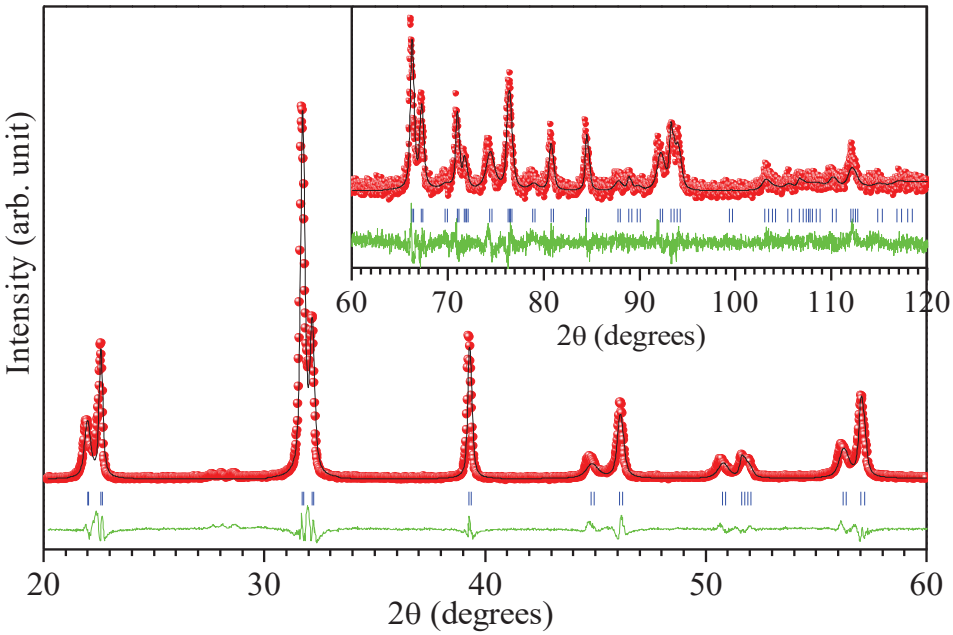

Fig.3.6. Experimentally observed (dots), theoretically calculated (continuous line) and their difference (continuous bottom line) profiles for (1-x)Bi($Ni_{1/2}Ti_{1/2}$)O_3-x$PbTiO_3$ with x=0.55 obtained after Rietveld analysis of the powder XRD data using tetragonal (P4mm) structure. The vertical tick-marks above the difference plot show the peak positions.

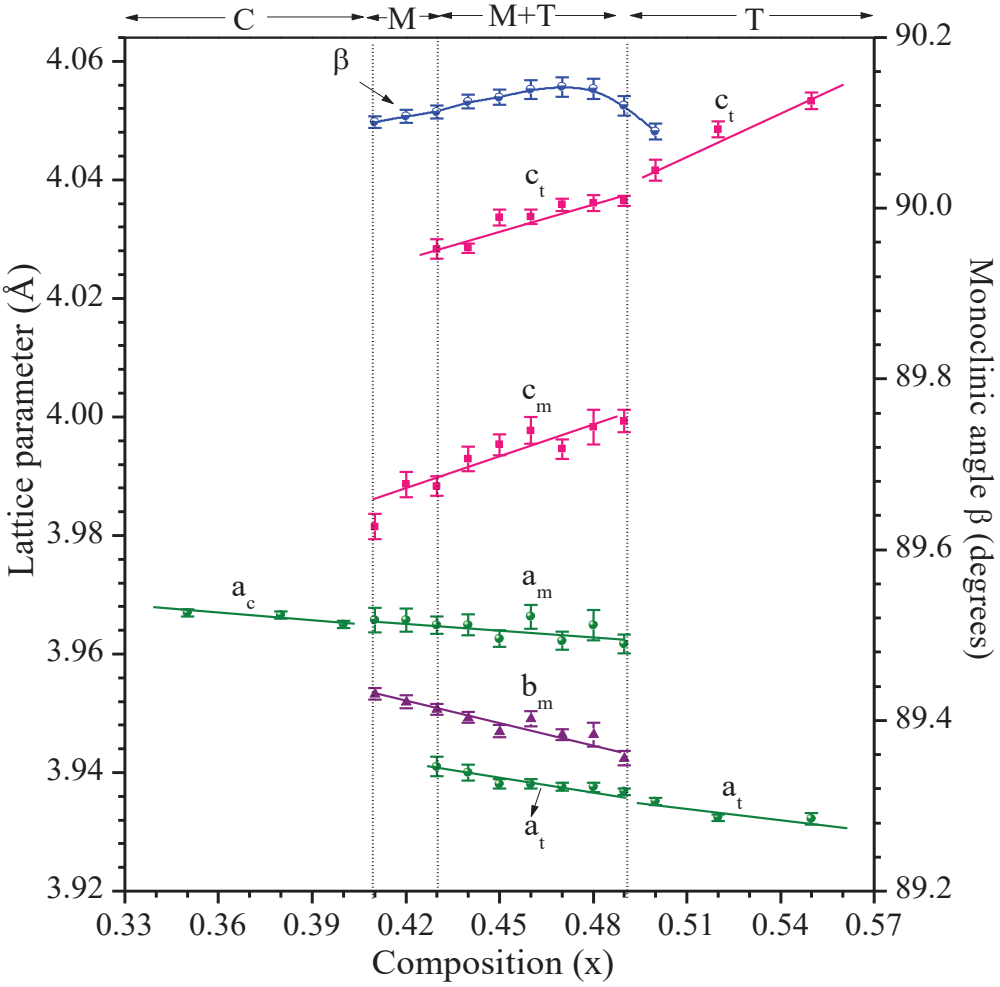

Fig.3.7 Variation of lattice parameters with composition for (1-x)$Bi(Ni_{1/2}Ti_{1/2})O_3$-x$PbTiO_3$ ceramics. The vertical dotted lines demarcate the stability region of various phases.

Table 3.1: Refined structural parameters for the single phase monoclinic (space group Pm) compositions with x=0.41 and 0.42.

(x)	Ions	*x*	*y*	*z*	Thermal parameters ($Å^2$)	Lattice Parameters (Å)
0.41	Bi/Pb	0.0	0.0	0.0	β_{11}=0.087(5), β_{22}=0.108(3), β_{33}=0.039(4)	a_m=3.9657(2)
(Pm)	Ni/Ti	0.52(1)	0.5	0.55(3)	Biso=0.04(3)	b_m=3.9533(3)
	O_I	0.44(3)	0.0	0.61(4)	Biso=0.15(2)	c_m=3.9815(6)
	O_{II}	0.41(1)	0.5	0.05(1)	Biso=0.10(3)	β=90.101(3)°
	O_{III}	-0.08(1)	0.5	0.58(4)	Biso=0.12(1)	
0.42	Bi/Pb	0.0	0.0	0.0	β_{11}=0.102(1), β_{22}=0.113(2), β_{33}= 0.045(3)	a_m=3.9657(3)
(Pm)	Ni/Ti	0.523(8)	0.5	0.553(4)	Biso=0.07(3)	b_m=3.9519(3)
	O_I	0.44(2)	0.0	0.61(3)	Biso=0.17(2)	c_m=3.9886(8)
	O_{II}	0.41(2)	0.5	0.05(2)	Biso=0.10(3)	β=90.108(1)°
	O_{III}	-0.05(3)	0.5	0.59(1)	Biso=0.13(1)	

Table 3.2: Refined structural parameters for the phase coexistence region with x=0.43-0.49 using monoclinic and tetragonal (Pm+P4mm) structures.

(x)	Ions	*x*	*y*	*z*	Thermal parameters ($Å^2$)	Lattice Parameters (Å)
0.43	Bi/Pb	0.0	0.0	0.0	β_{11}=0.081(1),β_{22}=0.10(8), β_{33}=0.052(4)	a_m=3.9649(5),
(Pm)	Ni/Ti	0.527(5)	0.50	0.548(2)	Biso=0.07(3)	b_m=3.9507(3)
	O_I	0.46(2)	0.0	0.61(8)	Biso=0.17(2)	c_m=3.9883(5)
	O_{II}	0.41(3)	0.5	0.09(1)	Biso=0.10(3)	β=90.113(4)°
	O_{III}	-0.02(2)	0.5	0.56(3)	Biso=0.13(1)	
(P4mm)	Bi/Pb	0.0	0.0	0.0	β_{11}=β_{22}=0.030(2), β_{33}=0.011(2)	a_t=3.9410(3)
	Ni/Ti	0.5	0.5	0.552(3)	Biso=0.15(1)	c_t=4.0283(5)
	O_I	0.5	0.5	0.13(1)	Biso=1.2(2)	
	O_{II}	0.5	0.0	0.651(7)	Biso=0.8(1)	
0.44	Bi/Pb	0.0	0.0	0.0	β_{11}=0.086(6),β_{22}=0.094(8),β_{33}= 0.051(5)	a_m=3.9648(5)
(Pm)	Ni/Ti	0.526(5)	0.0	0.550(5)	Biso=0.04(3)	b_m=3.9493(3)
	O_I	0.45(3)	0.0	0.60(3)	Biso=0.17(2)	c_m=3.9929(1)
	O_{II}	0.41(1)	0.5	0.07(1)	Biso=0.10(3)	β=90.125(2)°
	O_{III}	-0.07(1)	0.5	0.60(3)	Biso=0.13(1)	
(P4mm)	Bi/Pb	0.0	0.0	0.0	β_{11}=β_{22}=0.039(1),β_{33}=0.011(2)	a_t=3.9400(2)
	Ni/Ti	0.5	0.5	0.549(3)	Biso=0.15(1)	c_t= 4.0285(4)
	O_I	0.5	0.5	0.123(7)	Biso=1.2(2)	
	O_{II}	0.5	0.0	0.626(4)	Biso=0.8(1)	
0.45	Bi/Pb	0.0	0.0	0.0	β_{11}=0.079(5),β_{22}=0.098(6),β_{33}=0.054(2)	a_m=3.9626(4)
(Pm)	Ni/Ti	0.532(4)	0.5	0.548(3)	Biso=0.04(3)	b_m=3.9470(3)
	O_I	0.44(1)	0.0	0.62(1)	Biso=0.17(2)	c_m=3.9953(5)
	O_{II}	0.41(1)	0.5	0.08(1)	Biso=0.10(3)	β=90.130(3)°
	O_{III}	-0.06(3)	0.5	0.59(2)	Biso=0.13(1)	
(P4mm)	Bi/Pb	0.0	0.0	0.0	β_{11}=β_{22}=0.035(1),β_{33}=0.021(2)	a_t=3.9381(2)
	Ni/Ti	0.5	0.5	0.544(3)	Biso=0.19(2)	c_t=4.0336(4)
	O_I	0.5	0.5	0.171(8)	Biso=1.3(1)	
	O_{II}	0.5	0.0	0.645(5)	Biso=0.9(1)	

0.46	Bi/Pb	0.0	0.0	0.0	β_{11}=0.101(8),β_{22}=0.113(1),β_{33}=0.057(6)	a_m=3.9663(6)
(Pm)	Ni/Ti	0.532(8)	0.5	0.555(6)	Biso=0.04(3)	b_m=3.9491(4)
	O_I	0.44(3)	0.0	0.62(3)	Biso=0.17(2)	c_m=3.9977(8)
	O_{II}	0.41(1)	0.5	0.05(1)	Biso=0.10(3)	β=90.139(1)°
	O_{III}	-0.07(1)	0.5	0.58(4)	Biso=0.13(1)	
(P4mm)	Bi/Pb	0.0	0.0	0.0	β_{11}=β_{22}=0.041(1),β_{33}=0.018(1)	a_t=3.9381(2)
	Ni/Ti	0.5	0.5	0.542(2)	Biso=0.19(2)	c_t=4.0338(2)
	O_I	0.5	0.5	0.102(6)	Biso=1.3(1)	
	O_{II}	0.5	0.0	0.630(4)	Biso=0.9(1)	
0.47	Bi/Pb	0.0	0.0	0.0	β_{11}=0.084(2),β_{22}=0.10(1),β_{33}=0.076(1)	a_m=3.9622(5)
(Pm)	Ni/Ti	0.528(6)	0.0	0.551(5)	B_{iso}=0.04(3)	b_m=3.9464(3)
	O_I	0.45(2)	0.0	0.60(1)	B_{iso}=0.17(2)	c_m=3.9946(5)
	O_{II}	0.39(1)	0.5	0.08(1)	B_{iso}=0.10(3)	β=90.142(2)°
	O_{III}	-0.04(1)	0.5	0.55(2)	B_{iso}=0.13(1)	
(P4mm)	Bi/Pb	0.0	0.0	0.0	β_{11}=β_{22}=0.038(3),β_{33}=0.012(1)	a_t=3.9376(2)
	Ni/Ti	0.5	0.5	0.548(2)	B_{iso}=0.19(2)	c_t=4.0358(3)
	O_I	0.5	0.5	0.102(6)	B_{iso}=1.3(1)	
	O_{II}	0.5	0.0	0.639(3)	B_{iso}=0.9(1)	
0.48	Bi/Pb	0.0	0.0	0.0	β_{11}=0.068(2),β_{22}=0.13(1),β_{33}=0.056(7)	a_m=3.9649(3)
(Pm)	Ni/Ti	0.541(9)	0.5	0.554(8)	B_{iso}=0.04(3)	b_m=3.9464(7)
	O_I	0.44(3)	0.0	0.63(1)	B_{iso}=0.15(2)	c_m=3.9983(1)
	O_{II}	0.41(0)	0.5	0.05(2)	B_{iso}=0.10(3)	β=90.140(2)°
	O_{III}	-0.06(5)	0.5	0.56(3)	B_{iso}=0.12(2)	
(P4mm)	Bi/Pb	0.0	0.0	0.0	β_{11}=β_{22}=0.043(4),β_{33}=0.013(2)	a_t=3.9375(2)
	Ni/Ti	0.5	0.5	0.538(3)	B_{iso}=0.19(2)	c_t=4.0361(4)
	O_I	0.5	0.5	0.135(6)	B_{iso}=1.2(1)	
	O_{II}	0.5	0.0	0.638(4)	B_{iso}=0.8(1)	
0.49	Bi/Pb	0.0	0.0	0.0	β_{11}=0.081(6),β_{22}=0.124(4),β_{33}=0.073(3)	a_m=3.9617(5)
(Pm)	Ni/Ti	0.554(5)	0.5	0.552(5)	B_{iso}=0.04(3)	b_m=3.9424(4)
	O_I	0.43(2)	0.0	0.59(3)	B_{iso}=0.15(2)	c_m=3.9993(6)
	O_{II}	0.40(1)	0.5	0.08(1)	B_{iso}=0.10(3)	β=90.120(3)°
	O_{III}	-0.04(1)	0.5	0.57(4)	B_{iso}=0.12(2)	
(P4mm)	Bi/Pb	0.0	0.0	0.0	β_{11}=β_{22}=0.041(5),β_{33}=0.025(1)	a_t=3.9368(1)
	Ni/Ti	0.5	0.5	0.545(2)	B_{iso}=0.19(1)	c_t=4.0364(2)
	O_I	0.5	0.5	0.113(4)	B_{iso}=0.2(1)	
	O_{II}	0.5	0.0	0.634(2)	B_{iso}=0.2(0)	

Table 3.3: Refined structural parameters for the compositions with x=0.50, 0.52 to 0.55 using tetragonal (P4mm) structure.

(x)	Ions	*x*	*y*	*z*	Thermal parameters ($Å^2$)	Lattice Parameters (Å)
0.50	Bi/Pb	0.0	0.0	0.0	$\beta_{11}=\beta_{22}=0.041(5),\beta_{33}=0.028(1)$	$a_t=3.9351(3)$
(P4mm)	Ni/Ti	0.5	0.5	0.546(2)	$B_{iso}=0.3(1)$	$c_t=4.0416(2)$
	O_I	0.5	0.5	0.120(3)	$B_{iso}=0.2(1)$	
	O_{II}	0.5	0.0	0.629(3)	$B_{iso}=0.2(0)$	
0.52	Bi/Pb	0.0	0.0	0.0	$\beta_{11}=\beta_{22}=0.014(5),\beta_{33}=0.024(1)$	$a_t=3.9324(1)$
(P4mm)	Ni/Ti	0.5	0.5	0.543(2)	$B_{iso}=0.3(2)$	$c_t=4.0485(4)$
	O_I	0.5	0.5	0.116(3)	$B_{iso}=0.2(1)$	
	O_{II}	0.5	0.0	0.626(3)	$B_{iso}=0.2(0)$	
0.55	Bi/Pb	0.0	0.0	0.0	$\beta_{11}=\beta_{22}=0.039(1)$, $\beta_{33}=0.027(1)$	
(P4mm)	Ni/Ti	0.5	0.5	0.547(2)	$B_{iso}=0.3(2)$	$a_t=3.9322(1)$
	O_I	0.5	0.5	0.117(3)	$B_{iso}=0.2(1)$	$c_t=4.0533(3)$
	O_{II}	0.5	0.0	0.624(2)	$B_{iso}=0.2(0)$	

The refined structural parameters and the positional coordinates are listed in Table 3.1 for the single phase monoclinic (space group Pm) structure with x=0.41 and 0.42, Table 3.2 for the phase coexistence region with x=0.43-0.49 using monoclinic and tetragonal (Pm+P4mm) structures and Table 3.3 for the compositions with x=0.50, 0.52 to 0.55 using single phase tetragonal (P4mm) structure.

3.5.2.6. Variation of the (B-O) Bond Lengths with Composition

First-principles density functional theory (DFT) calculations by Qi et al. (2010) suggests that the tetragonality (c/a) is strongly coupled with the B-site cations displacement in Bi/Pb-based solid solutions and hence the nature of B-O bonding in ABO_3 perovskite. Variations in the bond lengths for the B-site (Ni/Ti) cations with apical and planer oxygen anions as the function of composition are shown in Figs.3.8(a,b,c). The (B-O) bond lengths calculated on the basis of Shannon-Prewitt ionic radii are shown by bold line in these figures. As can be seen from Fig.3.8(a), for the cubic compositions ($x \leq 0.40$), where the Wyckoff positions are same for all O ions, the calculated bond length is nearly equal to the experimental value, suggesting the ionic nature of the Ni/Ti-O bonds. In this case, we get six Ni/Ti-O bonds of same length. With increasing the PT content, the Ni/Ti-O bond lengths corresponding to monoclinic phase is splitted into five unequal parts as space group symmetry changes from cubic to monoclinic. Due to three different types of Wyckoff positions occupied by O ions, we get two Ni/Ti-O_I bonds of same length, two Ni/Ti-O_{II} and Ni/Ti-O_{III} bonds of unequal length as shown in Fig.3.8(b). This compositional region ($0.41 \leq x \leq 0.49$)

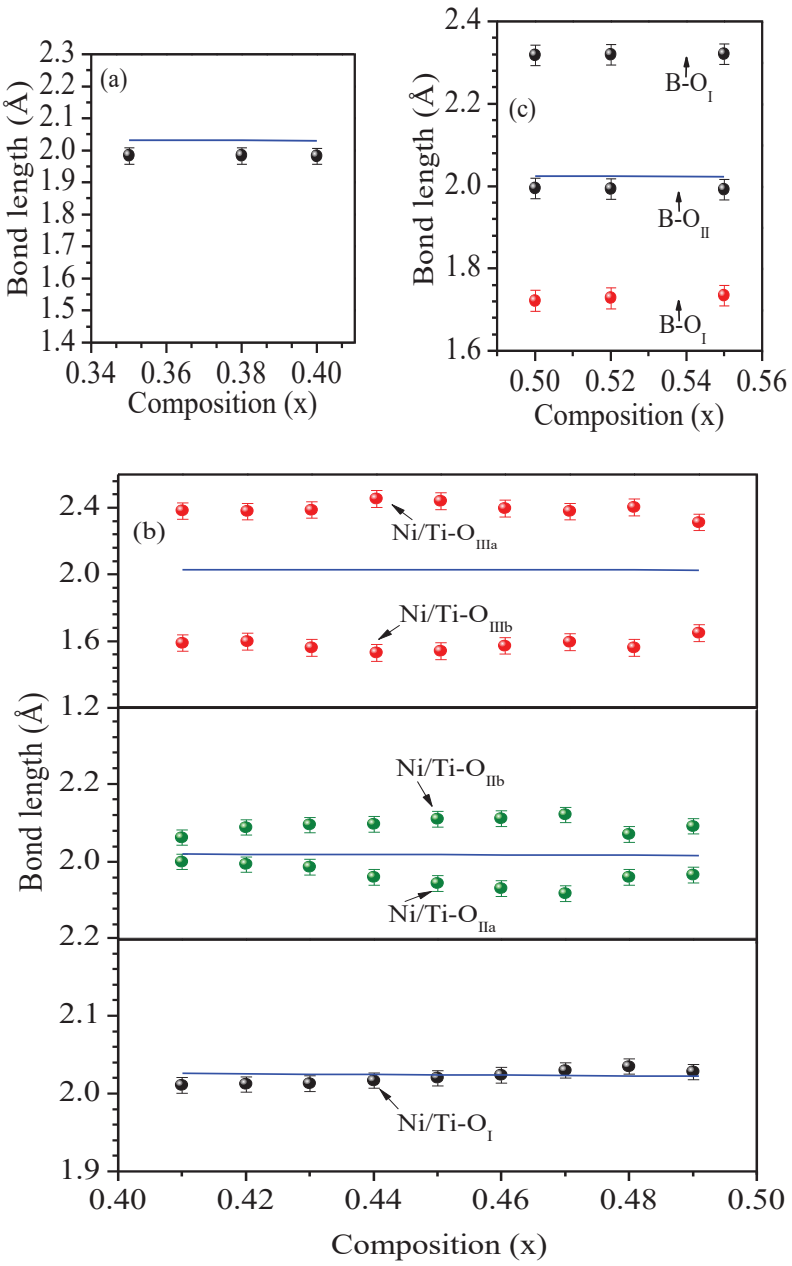

Fig.3.8 Variations of Ni/Ti–O (i.e., B-O) bond lengths for (a) cubic (x≤0.40), (b) monoclinic (0.41≤x≤0.49) and (c) tetragonal (x≤0.50) phases with composition obtained after Rietveld refinement. Solid (blue) line shows the bond lengths calculated using Shannon-Prewitt ionic radii.

Table 3.4: Ni/Ti-O bond lengths for BNT-PT solid solution obtained by using Rietveld refined structural parameters for the composition range $0.41 \leq x \leq 0.49$ with monoclinic structure (Pm).

(x)	Ni/Ti-O_I (Å)	Ni/Ti-O_{IIa} (Å)	Ni/Ti-O_{IIb} (Å)	Ni/Ti-O_{IIIa} (Å)	Ni/Ti-O_{IIIb} (Å)
0.41	2.011(5)	2.001(3)	2.063(1)	2.382(2)	1.590(2)
0.42	2.012(0)	1.994(1)	2.089(4)	2.379(2)	1.601(1)
0.43	2.013(2)	1.987(2)	2.095(4)	2.388(4)	1.561(6)
0.44	2.017(5)	1.961(2)	2.097(4)	2.454(8)	1.531(2)
0.45	2.020(5)	1.945(2)	2.110(1)	2.441(2)	1.541(1)
0.46	2.024(8)	1.932(0)	2.112(4)	2.398(6)	1.573(6)
0.47	2.030(2)	1.919(7)	2.092(3)	2.379(6)	1.649(3)
0.48	2.035(0)	1.961(5)	2.062(3)	2.403(0)	1.562(1)
0.49	2.028(1)	1.967(0)	2.120(4)	2.314(5)	1.596(6)

Table 3.5: Ni/Ti-O bond lengths for BNT-PT solid solution obtained by using Rietveld refined structural parameters for the tetragonal (P4mm) compositions with x=0.50, 0.52 and 0.55.

(x)	Ni/Ti-O_{Ia} (Å)	Ni/Ti-O_{Ib} (Å)	Ni/Ti-O_{II} (Å)
0.50	1.722(1)	2.318(1)	1.995(5)
0.52	1.728(2)	2.319(3)	1.994(6)
0.55	1.735(3)	2.325(1)	1.992(1)

corresponds to MPB region where the monoclinic phase is the major phase. Fig.3.8(c) depicts the variation of Ni/Ti-O bonds for tetragonal compositions with $x \geq 0.50$. Due to the availability of two different types of Wyckoff positions for O ions in tetragonal (P4mm) structure, four Ni/Ti-O_{II} bonds are same in length while two Ni/Ti-O_I bond lengths are unequal. In order to understand the nature of Ni/Ti-O bonding in BNT-PT solid solution, we compare the Ti-O bonds in $PbTiO_3$ with Ni/Ti-O bonds for various compositions of BNT-PT. Shirane et al. (1956) have reported three types of Ti-O bonds (Ti-O_{Ia}=1.78Å, Ti-O_{Ib}=2.38Å and Ti-O_{II}=1.98Å) in tetragonal $PbTiO_3$. The Ni/Ti-O bond lengths obtained by Rietveld refinement for BNT-PT come out to be 1.9836(1)Å, 1.9833(1)Å and 1.9825(1)Å for the cubic compositions with x=0.35, 0.38 and 0.40 respectively, which are comparable to the Ti-O_{II} bond length in $PbTiO_3$. The Ni/Ti-O bond lengths are listed in Table 3.4 for the MPB compositions in the composition range $0.41 \leq x \leq 0.49$ with major phase as monoclinic (Pm) structure. It is evident from Table 3.4 that Ni/Ti-O_I, Ni/Ti-O_{IIa} and Ni/Ti-O_{IIb} bonds are comparable to Ti-O_{II} bond length in $PbTiO_3$ and reveal the ionic nature. Ni/Ti-O_{IIIa} bond lengths in BNT-PT are comparable to the Ti-O_{Ib} bond length in $PbTiO_3$. However Ni/Ti-O_{IIIb} bond lengths are shorter than the bond lengths in $PbTiO_3$, as reported by Shirane et al. (1956) and calculated using Shannon-Prewitt radii (1969). If we consider the ionic nature of the bonds then all bond lengths should be equivalent in length, as has been observed in the case of cubic phase. This clearly indicates the partial covalent nature of Ni/Ti-O_{IIIb} bonds in BNT-PT solid solution. The Ni/Ti-O bond lengths obtained by Rietveld refinement of BNT-PT for the

tetragonal composition with x≥0.50 are listed in Table 3.5. It is evident from the Table 3.5 that Ni/Ti-O_{II} bond lengths are almost equal to the Ti-O_{II} bond length in $PbTiO_3$. Ni/Ti-O_{Ia} and Ni/Ti-O_{Ib} bond lengths in BNT-PT are slightly lower but comparable to Ti-O_I bond length in $PbTiO_3$. The above results suggest that the tetragonality in BNT-PT can be described in the similar manner as explained in the $PbTiO_3$. It is reported that [Cohen (1992); Cohen (2006)] in the pure $PbTiO_3$, the hybridization between $Ti^{4+}(3d^o)$ and $O^{2-}(2p)$ soften the short range repulsion and results the ferroelectricity.

3.6. Discussion

The results discussed in the above Sections confirm that the structure of the morphotropic phase for BNT-PT solid solution is monoclinic with space group Pm. In contrast, the symmetry of the MPB phase in multiferroic PFN-PT solid solution is monoclinic in the space group Cm [Singh et al. (2008)] whereas the multiferroic BF-PT solid solution exhibit monoclinic phase in the Cc space group [Bhattacharjee and Pandey (2010)]. The phase transition from tetragonal to rhombohedral phase is forbidden by the group-subgroup symmetry relationship and therefore requires the presence of some other phase (monoclinic) mediating between them. Stability of monoclinic phases in ferroelectric perovskites may be explained by considering eighth coefficient free energy in the expansion of Landau-Devonshire (LD) theory of ferroelectric homogeneous state [Vanderbilt and Cohen (2001)]. Ever since the discovery of the MPB in the PZT and similar solid solutions, it is believed that the coexistence of the rhombohedral and tetragonal phases, makes available total 14 (6 for tetragonal and 8 for

rhombohedral) orientational directions for the polarization, thereby maximizing the piezoelectric response [Park and Shrout (1997)]. Later on Noheda et al. (1999) discovered a monoclinic phase in the PZT system followed by the discovery of monoclinic phases in several other MPB solid solutions such as PMN-PT [Singh and Pandey (2001); Singh and Pandey (2003)], PZN-PT [Orauttapong et al. (2002)], $(PbSc_{1/2}Nb_{1/2}O_3)_{1-x}$-(PbTiO3)x [Haumont et al. (2003)], $BiScO_3$-$PbTiO_3$ [Chaigneau et al. (2007)] etc. First principles calculations [Fu and Cohen (2000)] suggested that rotation of polarization vector, in planes corresponding to the monoclinic phases observed in the MPB region, leads to ultra high electromechanical response. The polarization vector has more freedom to rotate in the monoclinic phase in comparison to the coexisting rhombohedral and tetragonal phases. Recently, it has been observed experimentally that significant domain wall and interphase boundary motion occurs in the MPB region and domain wall motion within the monoclinic phase has strong contribution to the electric field induced strain/piezoelectric response [Jones et al. (2012)]

Jin et al. (2003) have reported that conformal miniaturization of stress accommodating tetragonal/rhombohedral domains under the condition of low domain wall energy density can mimic the monoclinic symmetry as observed in the diffraction experiments. It is reported that for very low values of domain-wall energies the system transforms into a mixed adaptive state which is inhomogeneous on the nanoscale and homogeneous on the macroscale. Phase identification is usually carried out by the x-ray or neutron diffraction

experiments. Coherence length of these radiations is much larger than the conformally miniaturized nanodomains. Therefore, the resultant crystal structure identified by the intensity of diffraction profile provides the average structure of materials. As a consequence, the average diffraction profile of phase-coexisting nanoscale lamellar domains of rhombohedral and tetragonal phases (nanotwins) seems to be monoclinic phase in the diffraction profiles [Jin et al. (2003)]. A series of papers by Wang and co-workers [Jin et al. (2003); Rao W. F. and Wang (2007)] have also been shown that the monoclinic phase reported for the MPB can be expressed as conformally miniaturized stress accommodating tetragonal/rhombohedral domains. However, if one accepts these explanations then temperature dependence of the physical properties like elastic modulus and dielectric response should not show any anomaly corresponding to the phase transition from the monoclinic phase to the tetragonal phase [Singh et al. (2006); Singh et al. (2007)]. Filho et al. (2000) have reported that the tetragonal to monoclinic phase transition in $PbZr_{0.52}Ti_{0.48}O_3$ is also accompanied by the appearance of new Raman mode. If monoclinic symmetry is resulting due to miniaturization of tetragonal domains then one should not get any new Raman mode in the Raman spectra. Schonau et al. (2007) have performed a detailed synchrotron x-ray diffraction and transmission electron microscopic (TEM) studies on several compositions of PZT to correlate domain structure and appearance of monoclinic phase around MPB. The TEM studies reveal the miniaturization of the tetragonal domains while approaching to the MPB compositions. However due to experimental limitations, these workers could not

determine the symmetry of the miniaturized nanodomains. To reconcile all these observations with the appearance of the new Raman mode and anomalies in the temperature dependence of the physical properties corresponding to the tetragonal to monoclinic phase transition, we propose following model. As observed experimentally by Schonau et al. (2007) in TEM studies and also reported by Jin et al. (2003) and Rao and Wang (2007), one cannot disagree with the presence of the conformally miniaturized domains.

We believe that the conformal miniaturization of the rhombohedral/tetragonal domains in the compositions around MPB are responsible for the anisotropic broadening of the diffraction profiles of the rhombohedral and tetragonal phases, as one approaches the MPB. We observed significant anisotropic peak broadening in our BNT-PT samples for the compositions close to MPB. It is well known for the MPB systems like PZT [Noheda et al. (2000); Singh et al. (2007)] and PMN-PT [Singh et al. (2006)] that anisotropic broadening of the diffraction profiles is observed for the rhombohedral as well as tetragonal compositions close to the MPB. Consideration of monoclinic symmetry for the so-called rhombohedral compositions gives a better fit for the diffraction profiles in the Rietveld structure refinement. Such compositions do not show tetragonal to monoclinic transition with temperature. However, if the symmetry is indeed lowered to the monoclinic structure for the MPB phase, one observes tetragonal to monoclinic phase transition. It has been found in the MPB ceramics like PZT and PMN-PT that the tetragonal and rhombohedral compositions do not exhibit peak broadening of the

diffraction profiles away from the MPB where conformal miniaturization of domains is absent. As one approaches to MPB, gradually enhancing anisotropic peak broadening is observed for both the tetragonal and rhombohedral structures which eventually transforms to the monoclinic symmetry for the MPB compositions. This picture is also consistent with the results reported by Glazer et al. (2004) where they have shown that in the PZT system, the monoclinic character is present across the MPB with short range monoclinic ordering in the rhombohedral and tetragonal compositions which becomes long ranged in the MPB region. More theoretical and experimental investigations will be needed to further confirm this picture.

3.7. Summary

We have shown for the first time that the structure of the MPB phase in BNT-PT solid solution is monoclinic in the Pm space group. The structure of the compositions with $x \leq 0.40$ is cubic in the space group $Pm\bar{3}m$ and tetragonal in the space group P4mm for the compositions with $x \geq 0.50$. The MPB region exists in the composition range $0.41 \leq x \leq 0.49$. The compositions with x=0.41, 0.42 and 0.43 are nearly single phase monoclinic while the other compositions in the MPB region exhibit coexistence of minority tetragonal phase with space group P4mm. The correlation of anisotropic peak broadening and conformal miniaturization of rhombohedral/tetragonal domains in the vicinity of MPB with the appearance of monoclinic phase is also discussed.